

Journal of Biomedical Optics

BiomedicalOptics.SPIEDigitalLibrary.org

Kidney tumor staging using surface-enhanced Raman scattering

Sevda Mert
Emin Özbek
Alper Ötünçtemur
Mustafa Çulha

Kidney tumor staging using surface-enhanced Raman scattering

Sevda Mert,^a Emin Özbek,^b Alper Ötünçtemur,^b and Mustafa Çulha^{a,*}

^aYeditepe University, Department of Genetics and Bioengineering, Faculty of Engineering, Kayisdagi Street, Atasehir, Istanbul 34755, Turkey

^bOkmeydanı Education and Research Hospital, Department of Urology, Istanbul 34360, Turkey

Abstract. The detection of kidney cancers at an early stage is critical for diagnosis and therapy. Surface-enhanced Raman scattering (SERS) is investigated for early detection of cancer cases from biopsy samples. The colloidal silver nanoparticles as the SERS-active nanostructures are directly mixed with homogenized tissue samples. The SERS spectra from the normal and abnormal tissue samples collected from 40 cancer patients, 28 of them at T1 stage and 12 of them at T2–T3 stages, are analyzed using principal component analysis combined linear discriminant analysis with leave-one-out cross-validation method. It is found that the diagnosis sensitivity, specificity, and total accuracy of the approach can be as high as 100%. The results suggest that SERS can be used as a potential technique for the identification of the different tumor stages. © 2015 Society of Photo-Optical Instrumentation Engineers (SPIE) [DOI: 10.1117/1.JBO.20.4.047002]

Keywords: kidney tumor; renal cell carcinoma; surface-enhanced Raman scattering; principal component analysis; linear discriminant analysis.

Paper 140740RR received Nov. 11, 2014; accepted for publication Mar. 18, 2015; published online Apr. 9, 2015.

1 Introduction

Kidney cancer is almost 2% of all cancers worldwide, with its most common types being renal cell carcinoma (RCC) and transitional cell carcinoma (TCC). As the mortality rate due to kidney cancers increases by 2%–3% per decade, about 210,000 new cases are reported each year and over 100,000 patients die due to the disease.¹ Kidney cancer is diagnosed based on the information obtained from imaging techniques, biopsy examinations, and blood and urine testing. The imaging techniques include ultrasound, intravenous pyelogram, computed tomography (CT or CAT) scan, cystoscopy/nephro-ureteroscopy, and magnetic resonance imaging.

The commonly used treatment approach for kidney cancer is surgery including radical nephrectomy, partial nephrectomy (PN), laparoscopic nephrectomy, and robotic-assisted laparoscopic nephrectomy. According to the American Joint Committee on Cancer (AJCC), the most common staging system for kidney cancer is the association between tumor stage and tumor size as T1a ≤ 4 cm, T1b > 4 cm but ≤ 7 cm, T2a > 7 cm but ≤ 10 cm, T2b > 10 cm.² Tumor size is related to the recurrence rate, the survival rate, and the choice of clinical treatment method.^{3,4} Several studies have shown that subdividing the T1 tumor stage into T1a and T1b stages is beneficial for a better estimation of the survival rate in patients with tumors in the size of 4 cm or less.^{5,6} The lower recurrence rate after the PN process for the tumors < 4 cm was reported.⁷ In addition, the treatment of tumor sizes less than 4 cm showed no recurrence in the renal cell carcinoma patients followed for 61 months.⁸ It was reported that a four-fold increase in the local recurrence was observed with every 1-cm increase in the tumor size.⁹ The success rate of the cryoablation and radiofrequency ablation methods to treat kidney tumors is related to tumor sizes that are less than 4 cm.^{10–13} The recent reports have shown that the 5-year survival rate is

high in patients with RCC in the T1 early stage, and this rate is decreased in RCC patients as the cancer changes from T1 to T4 stages. The survival rate for patients is 94.9% in T1a, 92.6% in T1b, 85.4% in T2a, 70% in T2b, 64.7% in T3a, 54.7% in T3b, 17.9% in T3c, and 27.1% in T4 stage.² Hence, early detection and the prediction of the tumor stages increase the survival rate of kidney cancer patients with the prognostic morphologic parameters based on the microscopic morphology of a neoplasm with hematoxylin and eosin staining of cancer cell.¹⁴

Several spectroscopic techniques have been investigated to differentiate healthy and malignant tissues such as reflectance spectroscopy, fluorescence spectroscopy, light (elastic) scattering spectroscopy, infrared, and Raman spectroscopy.^{15–23} Among these techniques, Raman spectroscopy has some advantages, such as narrow spectral bandwidth, minimal interference from water, almost no photobleaching, and very rich spectral information to determine molecular changes in a sample compared to other spectroscopic techniques.

Surface-enhanced Raman scattering (SERS), a mode of Raman spectroscopy, has been investigated for its use in clinical applications to overcome the disadvantages of inherent inefficiency of Raman scattering and strong fluorescence background of biological samples. In an SERS experiment, a nanostructured noble metal substrate such as gold and silver is used to enhance the Raman scattering.²⁴ In addition to the advantageous features of Raman scattering such as fingerprinting property, narrow bandwidth and minimum sample preparation, a sensitivity increase in the Raman scattering down to a single molecule can be achieved.²⁵ Since the Raman spectrum from a molecule or molecular structure is its fingerprint, it can be used for label-free detection and identification of a molecule or molecular structure. In our previous studies, we demonstrated

*Address all correspondence to: Mustafa Çulha, E-mail: mculha@yeditepe.edu.tr

the feasibility of using SERS for tissue differentiation.^{26,27} The label-free detection and minimal sample preparation to obtain molecular information from a sample improves the efficiency in early detection of cancer.^{28–33} Recently, SERS-based diagnosis of cancer has been emerged as a powerful approach to detect many cancer types such as esophageal, nasopharyngeal, gastric, breast, ovarian, thyroid, bladder, lung, colorectal, and renal cancer.^{29,30,33–40}

In this study, SERS is evaluated for the identification and the classification of 40 normal and 40 abnormal pathologically evaluated tissue samples obtained from kidney cancer patients at different stages. The pattern recognition algorithm, a principal component analysis (PCA) combined with linear discriminant analysis (LDA), was used for the evaluation of the tissue samples. The accuracy of the classification results was predicted using leave-one-out cross-validation (LOO-CV) method. The results show that the classification of T1a, T1b, T2a, T2b, and T3a stage of renal cell carcinoma, and T3 stage of transitional cell carcinoma is possible with the SERS spectra obtained from tissue samples. This study demonstrates that SERS-based detection of early stage kidney cancer from tissue samples is a promising approach in clinical diagnosis.

2 Materials and Methods

2.1 Synthesis of Silver Nanoparticles

The Lee and Meisel method for preparation of colloidal silver nanoparticles (AgNPs) was used.⁴¹ Eighteen mg of AgNO₃ was dissolved in 100 mL of distilled water by stirring. Then the solution was heated to boiling, and 2 mL of 1% (w/v) trisodium citrate solution was dropped into this boiling solution. Finally, the solution was kept boiling until it was only half of the initial volume. The solution was concentrated by centrifugation at 5500 rpm for 30 min, and one-third of the supernatant was decanted to increase the final concentration of the AgNPs colloidal suspension to four times, which was called 4×. The maximum of the UV/visible spectrum from the resulting AgNP suspension was at 420 nm [Fig. 1(a)] indicating the average size of the AgNPs as 50 nm. The final density of the AgNPs in the 4× concentrated suspension was calculated as 2.08×10^{11} particles/mL.⁴²

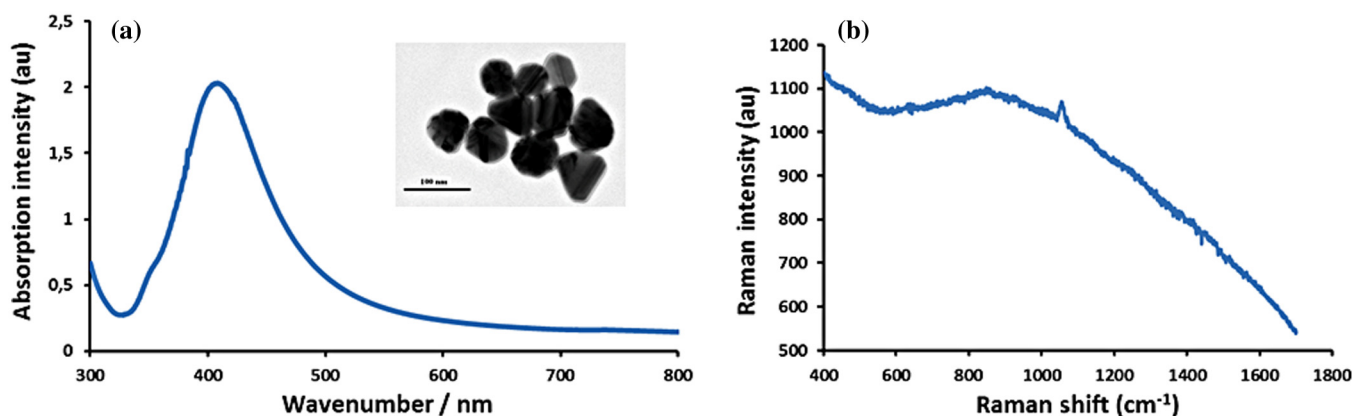


Fig. 1 (a) UV/visible absorption spectra of silver nanoparticle (AgNP) colloidal suspension. (b) Surface-enhanced Raman scattering (SERS) spectrum of colloidal AgNPs. The insert shows the transmission electron microscopy micrograph of AgNPs.

2.2 Kidney Cancer Tissue Sample

The biopsy samples of kidney tissues were obtained from the cancer patients with consent of the ethical approval from the Department of Urology at Okmeydani Education and Research Hospital. The tissue samples obtained during surgery were separated into two parts. One portion was saved for the histopathological examination, while the other half was stored at -80°C in plastic tubes until the sample preparation for the SERS measurements. The histopathological tumor staging was performed by a panel of pathologists. Table 1 shows the kidney tumors stages, the age, and the gender of the biopsied patients. For the SERS measurements, the sample preparation was performed using our previously reported method.²⁶ Briefly, a piece of tissue approximately in the size of $2 \times 2 \times 3 \text{ mm}^3$ was cut from sample tissue and tumor samples and placed in a mortar with 5 mL of liquid nitrogen to be crushed with a pestle. This crushed and liquefied tissue was mixed with 200 μL of the AgNP suspension. Then a 5 μL volume of this mixture was placed onto a CaF₂ slide, and each of the CaF₂ slides was dried in an inverted position under sterile conditions.⁴³ The average number of spectra collected on each tissue sample was 10 with three repeated Raman measurements. A total of 800 SERS spectra were acquired from 40 normal and 40 abnormal tissues, in which 280 SERS spectra were from T1 stage tumor tissues, 120 SERS spectra were from T2–T3 stage tumor tissues, and 400 SERS spectra were from the normal tissues.

2.3 Raman System and Surface-Enhanced Raman Scattering Measurements

A Renishaw InVia Reflex Raman microscopy system (Renishaw Plc., New Mills, Wotton-under-Edge, UK) equipped with an 830-nm diode was calibrated by using the silicon phonon mode at 520 cm^{-1} . The incident laser power was 3 mW on the sample, and the spectral data acquisition time was 10 s. The SERS spectra were acquired over a spectral range of $400 - 1800 \text{ cm}^{-1}$ with a 50× microscope objective (NA: 0.50). The SERS spectra were collected from randomly selected points on the sample using the “map image acquisition method” function in WIRE 2.0 software, and the WIRE 2.0 software carried out the spectral analyses.

Table 1 Histopathological tumor staging, age and gender of patients that tissues are biopsied.

SN	CT	TS	G	A
S1	RCC	T1b	F	48
S2	RCC	T1a	M	56
S3	RCC	T2b	M	67
S4	RCC	T1a	F	69
S5	TCC	T3	M	74
S6	RCC	T1b	M	64
S7	RCC	T2a	F	51
S8	RCC	T1b	F	65
S9	RCC	T1a	M	49
S10	RCC	T1a	M	71
S11	RCC	T1b	F	63
S12	RCC	T1b	M	48
S13	RCC	T1b	M	56
S14	RCC	T1a	M	61
S15	RCC	T1a	F	49
S16	RCC	T2a	M	65
S17	RCC	T1b	F	59
S18	RCC	T1b	F	62
S19	RCC	T2a	M	39
S20	TCC	T3	M	61
S21	RCC	T3a	M	71
S22	RCC	T1a	M	45
S23	RCC	T1a	M	58
S24	RCC	T1b	F	44
S25	RCC	T1b	M	62
S26	RCC	T3a	M	55
S27	RCC	T1b	M	67
S28	RCC	T1b	F	68
S29	RCC	T3a	M	71
S30	RCC	T3a	M	58
S31	RCC	T3a	M	61
S32	RCC	T1b	F	46
S33	RCC	T3a	M	60
S34	RCC	T1a	F	62

Table 1 (Continued).

SN	CT	TS	G	A
S35	RCC	T1b	M	59
S36	RCC	T1a	F	48
S37	RCC	T1a	M	64
S38	RCC	T1b	M	73
S39	RCC	T1b	F	56
S40	RCC	T1a	M	51

Note: SN: Sample number; CT: Cell type; TS: Tumor stage; G: Gender; A: Age.

2.4 Spectral Data Processing and Analysis

Each of randomly selected 10 SERS spectra obtained from each tissue sample was normalized to reduce the variations in the Raman intensity and to permit comparison of the spectral shapes. The spectral dataset was processed with the statistical package for the social science (SPSS) package (SPSS Inc., Chicago, Illinois), which contains PCA and LDA algorithms for statistical analysis to clarify the significant spectral characteristics of each tissue type and differentiate tissue types from each other for tumor stage identification. PCA was applied before LDA to reduce the number of dimensions ($d = 2009$) in the original high-dimensional dataset. To apply PCA, the spectral data observations having 2009 predictors were placed into a data matrix using 10 SERS spectra for each tissue sample. The eigenvalue decomposition was performed to the covariance matrix of the spectral data matrix. The resultant eigenvectors were obtained, and the original spectral dataset was projected into the new coordinate system defined by the principal directions of variance, called the principal components (PCs), which are the linear combination of the original data variables.⁴⁴ One way analysis of variance (ANOVA)^{45,46} is used to determine the most significant PCs ($p < 0.05$), then PCs were used in LDA to generate diagnostic algorithms for the classification of the tumors with different stages. LOO-CV⁴⁷ methodology was applied to demonstrate the accuracy of the classification.^{48,49} The significant differences in the Raman peak intensities for each tissue class were obtained by applying one-way ANOVA with a Tukey *post-hoc* test (significance level $p < 0.05$).^{45,50,51}

3 Results and Discussion

3.1 Spectral Characteristics of Normal and Cancerous Kidney Tissues

SERS spectra were recorded from each type of normal and cancerous tissues. The mapping method of WIRE 2.0 software was applied to collect at least 10 spectra from randomly selected points from the dried sample composed of homogenized tissue and the colloidal AgNPs. The histopathologic stages of the cancer tissues according to TNM (tumor, node, and metastasis) classification were T1a, T1b, T2a, T2b, and T3a for RCC and T3 for TCC. The mean spectra of RCC tissue from the different stages T1a (120), T1b (160), T2a (30), T2b (10), and T3a (60) with the mean spectra of TCC tissue from the T3 (20) stage tumor and the mean spectra of normal tissues (400)

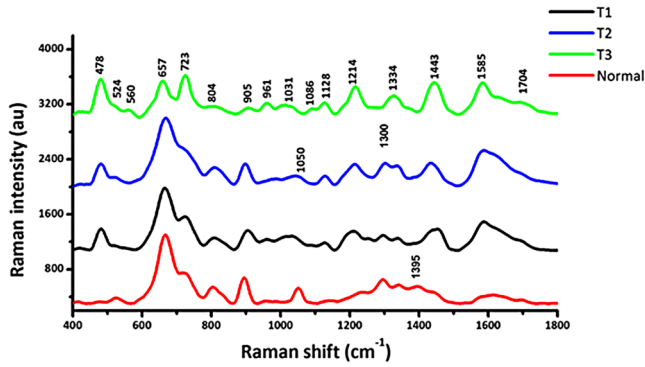


Fig. 2 Mean SERS spectra obtained from normal tissues and cancerous tissues at T1 (T1a-T1b), T2 (T2a-T2b), T3 (T3a) stages.

were normalized to the integrated area under the curve in the range of $400 - 1800 \text{ cm}^{-1}$ to enable a better comparison of the spectral shapes and the relative peak intensities among on the spectra obtained from the different tissue samples. Figure 2 shows the comparison of the normalized average SERS spectra

acquired from the normal tissues and cancerous tissues at T1 (T1a-T1b), T2 (T2a-T2b), and T3 (T3a) stages. The major SERS peaks, which can be attributed to biochemical constituents such as nucleic acids ($478, 560, 723, 1086,$ and 1334 cm^{-1}), proteins ($524, 657, 804, 1031, 1050, 1214, 1300, 1395, 1443, 1585,$ and 1704 cm^{-1}), carbohydrates (905 cm^{-1}), and lipids ($961, 1128,$ and 1443 cm^{-1}), were obtained from normal and abnormal tissue subjects. The tentative assignments for the observed SERS bands are listed in Table 2 in order to understand the possible molecular basis of the changes in the tissue samples based on previously reported studies in the literature.^{40,52-63} Figure 3 shows that the normalized intensities of SERS peaks at $478, 560, 723, 961, 1031, 1086, 1128, 1214, 1334, 1443, 1585,$ and 1704 cm^{-1} are higher for the tumor tissues than those of the normal tissues, while the intensities of the SERS bands at $657, 1050,$ and 1395 cm^{-1} are higher on the spectra obtained from the normal tissues. The statistical significance of differences in the peak intensities between the different pathology groups and normal group was identified using one-way ANOVA with a Tukey *post-hoc* test (significance level $p < 0.05$).

Table 2 Peak positions and tentative assignment of Raman bands.^{40,52-63}

Peak positions (cm^{-1})				
Normal	T1 stage	T2 stage	T3 stage	Major assignment
—	478	478	478	DNA/ RNA
524	524	523	524	S—S disulfide stretching in proteins
—	—	—	560	G/ T/ U
666	662	664	657	C—S stretching mode of Cys
726	724	722	723	A (ring breathing mode of DNA/RNA bases)
804	807	805	804	Asn
901	902	904	905	Pro/Val/Glycogen
962	960	963	961	Cholesterol
1031	1030	1033	1031	C—H in-plane bending mode of Phe
1050	1048	1048	1050	C—O stretching, C—N stretching in proteins
—	—	—	1086	Phosphodiester groups in nucleic acids
1129	1128	1129	1128	C—C stretching mode of lipids
1216	1214	1214	1214	C—C ₆ —H ₅ stretching mode in Tyr and Phe
1298	1298	1300	1300	Ser/Glu/Lipids
1335	1337	1335	1334	DNA—purine bases/ Collagen
1395	—	—	—	Protein
1445	1445	1443	1443	Collagen and phospholipids
1586	1585	1584	1585	C=C bending mode of Phe
1704	1704	1704	1704	Phe

Note: A-Adenine; Asn-Asparaginase; Cys-Cysteine; Glu-Glutamate; G-Guanine; Ser-Serine; T-Thymine; Tyr- Tyrosine; Phe-Phenylalanine; Pro-Proline; U-Uracil; Val-Valine.

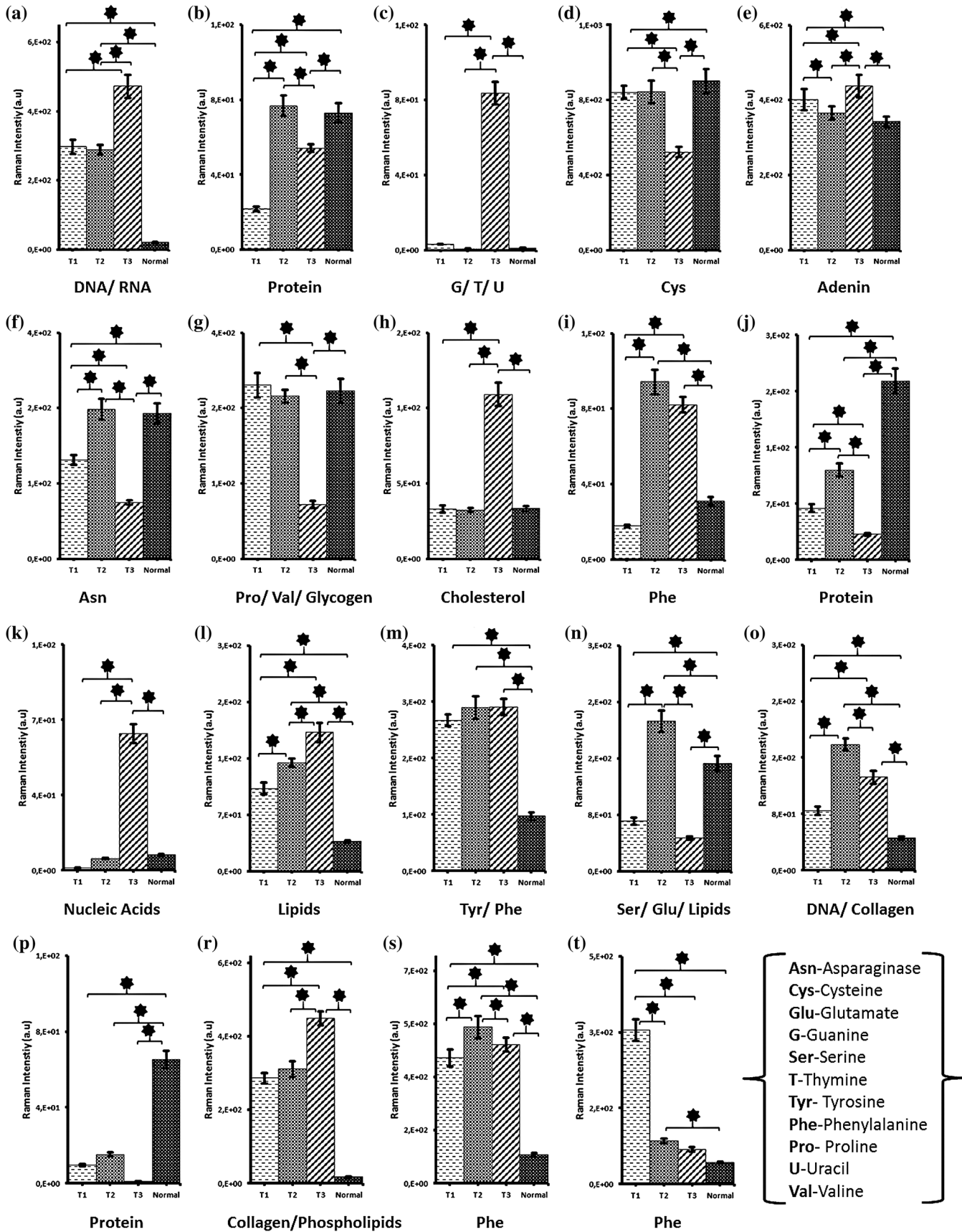


Fig. 3 Column plots of 19 significant SERS peak intensities for the four tissue types (normal, T1, T2, and T3 stage cancers) (a) 478, (b) 524, (c) 560, (d) 657, (e) 723, (f) 804, (g) 905, (h) 961, (i) 1031, (j) 1050, (k) 1086, (l) 1128, (m) 1214, (n) 1300, (o) 1334, (p) 1395, (r) 1443, (s) 1585, (t) 1704 cm^{-1} . Error bars represent the standard deviation for SERS spectra obtained from each type of tissue. *Significantly different from each other [$P < 0.05$, one-way analysis of variance (ANOVA) with Tukey's HSD *post-hoc* test].

The selected spectral intensities, where the standard deviations do not overlap, were displayed in Fig. 3, and the differences are thus significant and reproducible. The significant decrease and increase for biomolecules is relative to the total Raman active components in the different tissue groups. These spectral intensity differences for the different pathological tissues and normal tissues could be evaluated for a better understanding of molecular changes between malignant and normal tissue types. The peak intensities at 478, 723, and 1334 cm^{-1} , primarily related to nucleic acids, were found to be increased in the cancer groups, indicating the uncontrolled fast replication of DNA in cancer cells. This is associated with the increased nucleic acid content in cancer cells. The band intensities at 560 and 1086 cm^{-1} were higher on the spectra obtained from tissues at the T3 stage than the normal and T1–T2 stages.⁶⁴ The band at 961 cm^{-1} , attributed to cholesterol, is more intense on the spectra obtained from the tumors, especially at the T3 stage. This increased intensity may be attributed to an increased cholesterol synthesis in cancer tissues.^{65,66} Phenylalanine-related bands at 1031, 1214, 1585, and 1704 cm^{-1} in cancer groups are associated with increased phenylalanine contents relative to the total Raman-active components in cancer tissues.^{58,63} In a study, it was found that the uptake rate of amino acids in cancer was higher.⁶⁷ The increased band intensity at 1128 cm^{-1} in the cancer groups may be attributed to the increased lipid concentration in the tumors. The studies comprising the high levels of fatty acid synthesis related to the tumor aggressiveness are consistent with our study results.^{68–70} The band at 1443 cm^{-1} , which is probably characteristic of collagen and phospholipids, shows a higher intense signal in malignant tissues and indicates that the collagen synthesis significantly increased in the cancerous tissues.⁷¹ The bands at 657, 1050, and 1395 cm^{-1} , more intense in the normal tissue, are assigned to proteins, and the bands at 524, 804, and 1300 cm^{-1} , probably originating from proteins or lipids, were more intense in the normal tissues than the tumors at the T1 and T3 stages, even though it was the most intense on the spectrum from the cancerous tissue at the T2 stage. Note that there is a possibility that more than one band's vibrations might contribute to the band observed on the spectra. In addition, the intensity of the band at 905 cm^{-1} , associated with protein or glycogen, was higher on the spectra obtained from the normal tissues than that of the tumor at the T3 stage. However, the highest band intensity at 905 cm^{-1} was obtained from tumors at the T1 and T2 stages.

3.2 PCA-LDA as Diagnostic Algorithms

Renal cell carcinoma staging has been used as a significant prognostic factor for kidney cancer patients because the survival rate of patients with renal cancer is reduced from the early stage to the late stage. The PCA-LDA model was built to predict the classification of tissue types and to improve the diagnostic utility of kidney cancer patients. The SERS spectra acquired from normal and abnormal tissues were processed in SPSS software package (SPSS Inc., Chicago, Illinois) for PCA-LDA analysis after the intensity of the spectra was scaled within a similar range using the min–max normalization method to compare the relative peak intensities among the normal tissue and tumor stages in a more precise manner. The significant PCs obtained using one-way ANOVA comparison test ($p < 0.05$) was used in LDA to generate a diagnostic assay. The scatter plot of the posterior probabilities based on the linear discriminant scores of the normal and the cancerous tissues using the PCA-LDA

diagnostic algorithm is provided in Fig. 4. Each dot on the plot is associated with the SERS spectra acquired from each type of tissue. The LDA scatter plot of the classification model developed to differentiate the cancerous and the normal tissue samples shows a good discrimination among the normal and abnormal tissues at the different tumor stages. The discrimination results based on SERS spectra using a leave one out-cross validation method to evaluate the performance of the PCA-LDA models for the classification of different tumor stages in terms of sensitivity, specificity and 95% confidence interval of accuracy was displayed in Fig. 5. The RCC tumors at T1a stage related to PCs, which were subtracted from SERS spectra, were well differentiated from RCC tumors at T1b, T2a, T2b, and T3a stages, TCC tumors at T3 stage and the normal tissues with the diagnostic sensitivities of 100%, 100%, 65%, 100%, 89%, and 65%, the specificities of 100% from all types of tumor stages and 70% from the normal subjects, and the accuracy of 100%, 100%, 88%, 93%, 100%, and 69%, respectively. The discrimination results of the diagnostic combinations of RCC tumors at T1b stage versus T2a, T2b, and T3a stages, TCC tumors at T3 stage and normal tissues, and RCC tumors at T2a stage versus RCC tumors at T2b, T3a stages, TCC tumors at T3 stage and the normal tissues were achieved with a sensitivity, specificity, and accuracy of 100% while the posterior probabilities of RCC tumors at T2b stage versus RCC tumors at T3a stage, TCC tumors at T3 stage and normal tissues were obtained with sensitivities of 88%, 100%, and 80%, specificities of 43%, 100%, and 84%, and accuracies of 57%, 100%, and 83%, respectively. The RCC tumors at the T3a stage versus normal tissues were diagnosed with a sensitivity, specificity, and accuracy of 100%, and TCC tumors at the T3 stage were classified with a sensitivity of 100% and 70%, a specificity of 98% and 60%, and an accuracy of 98% and 62%, respectively.

The tumors at the T1, T2, and T3 stages with normal tissues were also differentiated using PCA-LDA models of the spectral

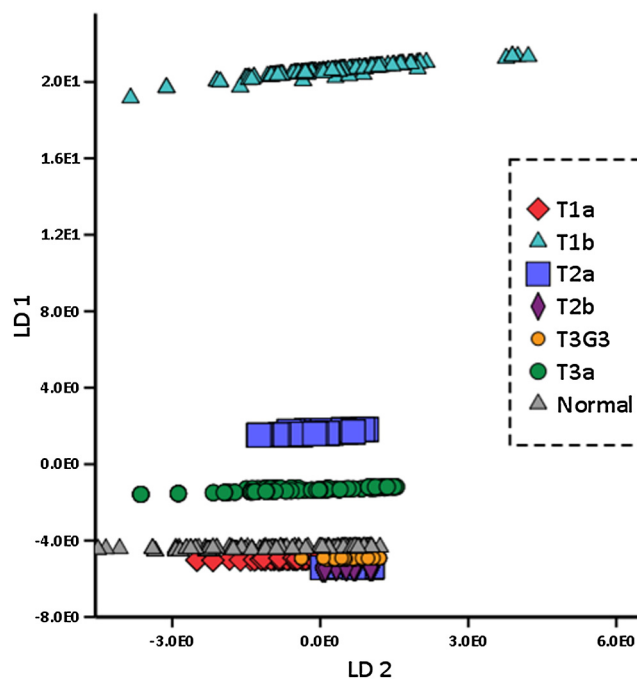


Fig. 4 Scatter plot of posterior probabilities for classification of normal tissues and tumors.

	T1b	T2a	T2b	T3	T3a	Normal
T1a tumor stage (RCC)	100	100	65	89	100	65
	100	100	100	100	100	70
	100	100	88	93	100	69
T1b tumor stage (RCC)	100	100	100	100	100	100
	100	100	100	100	100	100
	100	100	100	100	100	100
T2a tumor stage (RCC)	100	100	100	100	100	100
	100	100	100	100	100	100
	100	100	100	100	100	100
T2b tumor stage (RCC)	88	100	80			
	43	100	84			
	57	100	83			
T3 tumor stage (TCC)	100	70				
	98	60				
	98	62				
T3a tumor stage (RCC)	100					
	100					
	100					
Sensitivity %						
Specificity %						
Accuracy %						

Fig. 5 Leave-one-out cross-validation (LOO-CV) classification results of normal tissues and tumor tissues (T1a, T1b, T2a, T2b, and T3a stages of RCC; T3 stage of TCC).

data obtained from the normal and the abnormal tissue samples. As compared to the classification results in Fig. 5, Fig. 6 shows a better discrimination among the different tissue classes with a diagnostic sensitivity of 89%, 96%, 94%, 70%, 97%, and 98%, specificity of 100%, 100%, 96%, 83%, 94%, and 77%, and accuracy of 99%, 97%, 95%, 81%, 95%, and 85%, respectively, for the classification between T1 and T2 stage cancers; T1 and T3 stage cancers; T1 stage cancer and normal tissues; T2 and T3 stage cancers; T2 stage cancer and normal groups; T3 stage cancer and normal tissue, respectively. The classification of tumors at the advanced stages (T2–T3), at the early stage (T1), and for normal tissues was obtained with sensitivities of 93% and 100%, specificities of 98% and 86%, and accuracies of 91%, and 90%, respectively, indicating that the classification of normal tissues, early stage tumors, and advanced stage tumors is possible with a high diagnostic efficacy.

The three-dimensional scatter plot of the diagnostic probabilities of LD1, LD2, and LD3 discriminants were shown in Fig. 7, illustrating a good classification among the different tumor stages and the normal tissue groups. The diagnostic performance of PCA-LDA models on the classification of tissue types has been acquired with an improved accuracy by the selection of significant PCs and different Raman bands ($p < 0.05$).

4 Conclusions

The differences in the biochemical components of normal and cancer tissues are reflected on the SERS spectra, which can be used in PCA-LDA multivariate statistical models for the tissue differentiation. The differentiation of the tumors at different stages and the normal tissues with a sensitivity of 89%, 96%, 94%, 70%, 97%, and 98%, a specificity of 100%, 100%, 96%, 83%, 94%, and 77%, and an accuracy of 99%, 97%, 95%, 81%,

	T1 (T1a-T1b)	T2 (T2a-T2b)	T3 (T3a)	T2+T3 (Advanced stage)
Normal	94	97	98	98
	96	94	77	86
	95	95	85	90
T1 (T1a-T1b)		89	96	93
		100	100	100
		85	97	91
T2 (T2a-T2b)			70	Sensitivity %
			83	Specificity %
			81	Accuracy %

Fig. 6 LOO-CV classification results of normal tissues and tumors at T1, T2, and T3 stages.

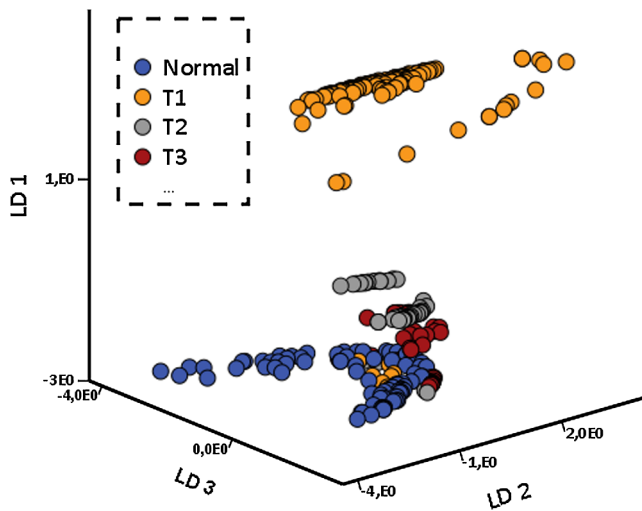


Fig. 7 Three-dimensional (3-D) scatter plot of diagnostic probabilities of normal tissues and tumors at T1, T2, and T3 stages.

95%, and 85% between T1 and T2 stages; T1 and T3 stages; T1 stages and normal; T2 and T3 stages; T2 stages and normal; and T3 stages and normal tissue, respectively, has been successfully demonstrated using PCA-LDA. The diagnostic discrimination of tumors at advanced (T2–T3) stages against the early stage (T1) and normal tissues resulted in sensitivities of 93% and 100%, specificities of 98% and 86%, and accuracies of 91% and 90%, respectively.

In conclusion, the SERS has the ability to differentiate the early stage kidney cancers, T1, and advanced stage kidney cancer, T2–T3, and normal tissues, using PCA-LDA diagnostic classification algorithms. The results suggest that the SERS spectra from tissue samples can be used to reach a clinical decision for the stage determination of kidney cancers.

Acknowledgments

We acknowledge the support from the Scientific and Technological Research Council of Turkey (TUBITAK) and Yeditepe University.

References

1. R. Siegel et al., "Cancer statistics, 2014," *CA Cancer J. Clin.* **64**(1), 9–29 (2014).
2. S. B. Edge et al., *AJCC Cancer Staging Manual*, Springer, New York (2010).
3. D. A. Levy et al., "Stage specific guidelines for surveillance after radical nephrectomy for local renal cell carcinoma," *J. Urol.* **159**(4), 1163–1167 (1998).
4. J. S. Lam et al., "Surveillance following radical or partial nephrectomy for renal cell carcinoma," *Curr. Urol. Rep.* **6**(1), 7–18 (2005).
5. K. S. Hafez, A. F. Fergany, and A. C. Novick, "Nephron sparing surgery for localized renal cell carcinoma: impact of tumor size on patient survival, tumor recurrence and TNM staging," *J. Urol.* **162**(6), 1930–1933 (1999).
6. J.-J. Patard et al., "Safety and efficacy of partial nephrectomy for all T1 tumors based on an international multicenter experience," *J. Urol.* **171**(6), 2181–2185 (2004).
7. H. Van Poppel and S. Joniau, "How important are surgical margins in nephron-sparing surgery?," *Eur. Urol. Suppl.* **6**(8), 533–539 (2007).
8. R. J. Zagoria et al., "Long-term outcomes after percutaneous radiofrequency ablation for renal cell carcinoma," *Urology* **77**(6), 1393–1397 (2011).
9. M. Tsivian et al., "Tumor size and endophytic growth pattern affect recurrence rates after laparoscopic renal cryoablation," *Urology* **75**(2), 307–310 (2010).
10. C. T. Nguyen, S. C. Campbell, and A. C. Novick, "Choice of operation for clinically localized renal tumor," *Urol. Clin. North Am.* **35**(4), 645–655 (2008).
11. D. S. Lehman et al., "First prize (tie): laparoscopic renal cryoablation: efficacy and complications for larger renal masses," *J. Endourol.* **22**(6), 1123–1128 (2008).
12. C. C. Wen and S. Y. Nakada, "Energy ablative techniques for treatment of small renal tumors," *Curr. Opin. Urol.* **16**(5), 321–326 (2006).

13. D. A. Gervais et al., "Radiofrequency ablation of renal cell carcinoma: part I, Indications, results, and role in patient management over a 6-year period and ablation of 100 tumors," *Am. J. Roentgenol.* **185**(1), 64–71 (2005).
14. S. A. Fuhrman, L. C. Lasky, and C. Limas, "Prognostic significance of morphologic parameters in renal cell carcinoma," *Am. J. Surg. Pathol.* **6**(7), 655–664 (1982).
15. K. Bensalah et al., "Optical reflectance spectroscopy to differentiate renal tumor from normal parenchyma," *J. Urol.* **179**(5), 2010–2013 (2008).
16. D. J. Parekh, W.-C. Lin, and S. D. Herrell, "Optical spectroscopy characteristics can differentiate benign and malignant renal tissues: a potentially useful modality," *J. Urol.* **174**(5), 1754–1758 (2005).
17. S. G. Vari and W. S. Grundfest, "Method for determining the biodistribution of substances using fluorescence spectroscopy," U.S. Patent No. 5,377,676 (1995).
18. Z. Volynskaya et al., "Diagnosing breast cancer using diffuse reflectance spectroscopy and intrinsic fluorescence spectroscopy," *J. Biomed. Opt.* **13**(2), 024012 (2008).
19. J. R. Mourant et al., "Spectroscopic diagnosis of bladder cancer with elastic light scattering," *Lasers Surg. Med.* **17**(4), 350–357 (1995).
20. K. Bensalah et al., "Raman spectroscopy: a novel experimental approach to evaluating renal tumours," *Eur. Urol.* **58**(4), 602–608 (2010).
21. B. W. De Jong et al., "Discrimination between nontumor bladder tissue and tumor by Raman spectroscopy," *Anal. Chem.* **78**(22), 7761–7769 (2006).
22. C. A. Lieber and M. H. Kabeer, "Characterization of pediatric Wilms' tumor using Raman and fluorescence spectroscopies," *J. Pediatr. Surg.* **45**(3), 549–554 (2010).
23. C. Krafft et al., "Disease recognition by infrared and Raman spectroscopy," *J. Biophotonics* **2**(1–2), 13–28 (2009).
24. D. L. Jeanmaire and R. P. Van Duyne, "Surface Raman spectroelectrochemistry: Part I. Heterocyclic, aromatic, and aliphatic amines adsorbed on the anodized silver electrode," *J. Electroanal. Chem. Interfacial Electrochem.* **84**(1), 1–20 (1977).
25. K. Kneipp et al., "Single molecule detection using surface-enhanced Raman scattering (SERS)," *Phys. Rev. Lett.* **78**(9), 1667 (1997).
26. Ö. Aydin et al., "Differentiation of healthy brain tissue and tumors using surface-enhanced Raman scattering," *Appl. Spectrosc.* **63**(10), 1095–1100 (2009).
27. Ö. Aydin et al., "Surface-enhanced Raman scattering of rat tissues," *Appl. Spectrosc.* **63**(6), 662–668 (2009).
28. J. Lin et al., "A novel blood plasma analysis technique combining membrane electrophoresis with silver nanoparticle-based SERS spectroscopy for potential applications in noninvasive cancer detection," *Nanomed. Nanotechnol. Biol. Med.* **7**(5), 655–663 (2011).
29. D. Lin et al., "Colorectal cancer detection by gold nanoparticle based surface-enhanced Raman spectroscopy of blood serum and statistical analysis," *Opt. Express* **19**(14), 13565–13577 (2011).
30. S. Feng et al., "Nasopharyngeal cancer detection based on blood plasma surface-enhanced Raman spectroscopy and multivariate analysis," *Biosens. Bioelectron.* **25**(11), 2414–2419 (2010).
31. D. Lin et al., "Label-free blood plasma test based on surface-enhanced Raman scattering for tumor stages detection in nasopharyngeal cancer," *Sci. Rep.* **4**(4751), 1–4 (2014).
32. S. Feng et al., "Blood plasma surface-enhanced Raman spectroscopy for non-invasive optical detection of cervical cancer," *Analyst* **138**(14), 3967–3974 (2013).
33. Z. Li et al., "Surface-enhanced Raman spectroscopy for differentiation between benign and malignant thyroid tissues," *Laser Phys. Lett.* **11**(4), 045602 (2014).
34. S. Feng et al., "Esophageal cancer detection based on tissue surface-enhanced Raman spectroscopy and multivariate analysis," *Appl. Phys. Lett.* **102**(4), 043702 (2013).
35. S. Feng et al., "Gastric cancer detection based on blood plasma surface-enhanced Raman spectroscopy excited by polarized laser light," *Biosens. Bioelectron.* **26**(7), 3167–3174 (2011).
36. Y. Li et al., "Simultaneous SERS detection and imaging of two biomarkers on the cancer cell surface by self-assembly of branched DNA-gold nanoaggregates," *Chem. Commun.* **50**(69), 9907–9909 (2014).
37. S. Boca-Farcau et al., "Folic acid-conjugated, SERS-labeled silver nanotriangles for multimodal detection and targeted photothermal treatment on human ovarian cancer cells," *Mol. Pharm.* **11**(2), 391–399 (2014).
38. Y. Liu et al., "Fabrication of silver ordered nanoarrays SERS-active substrates and their applications in bladder cancer cells detection," *Spectrosc. Spectral Anal.* **32**(2), 386–390 (2012).
39. X. Li, T. Yang, and J. Lin, "Spectral analysis of human saliva for detection of lung cancer using surface-enhanced Raman spectroscopy," *J. Biomed. Opt.* **17**(3), 0370031–0370035 (2012).
40. S. Mert and M. Çulha, "Surface-enhanced Raman scattering-based detection of cancerous renal cells," *Appl. Spectrosc.* **68**(6), 617–624 (2014).
41. P. Lee and D. Meisel, "Adsorption and surface-enhanced Raman of dyes on silver and gold sols," *J. Phys. Chem.* **86**(17), 3391–3395 (1982).
42. D. Paramelle et al., "A rapid method to estimate the concentration of citrate capped silver nanoparticles from UV-visible light spectra," *Analyst* **139**(19), 4855–4861 (2014).
43. S. Keskin and M. Çulha, "Label-free detection of proteins from dried-suspended droplets using surface enhanced Raman scattering," *Analyst* **137**(11), 2651–2657 (2012).
44. I. Jolliffe, *Principal Component Analysis*, Springer, United States (2002).
45. M. S. Bergholt et al., "Characterizing variability in in vivo Raman spectra of different anatomical locations in the upper gastrointestinal tract toward cancer detection," *J. Biomed. Opt.* **16**(3), 037003 (2011).
46. R. Bender and S. Lange, "Adjusting for multiple testing: when and how?," *J. Clin. Epidemiol.* **54**(4), 343–349 (2001).
47. S. Teh et al., "Diagnostic potential of near-infrared Raman spectroscopy in the stomach: differentiating dysplasia from normal tissue," *Br. J. Cancer* **98**(2), 457–465 (2008).
48. M. Li and B. Yuan, "2D-LDA: a statistical linear discriminant analysis for image matrix," *Pattern Recognit. Lett.* **26**(5), 527–532 (2005).
49. J. Shao, "Linear model selection by cross-validation," *J. Am. Stat. Assoc.* **88**(422), 486–494 (1993).
50. G. M. O'Regan et al., "Raman profiles of the stratum corneum define 3 filaggrin genotype-determined atopic dermatitis endophenotypes," *J. Allergy Clin. Immunol.* **126**(3), 574–580, e571 (2010).
51. R. Goswami et al., "Prevalence of thyroid autoimmunity in sporadic idiopathic hypoparathyroidism in comparison to type 1 diabetes and premature ovarian failure," *J. Clin. Endocrinol. Metab.* **91**(11), 4256–4259 (2006).
52. N. Stone et al., "Raman spectroscopy for identification of epithelial cancers," *Faraday Discuss.* **126**, 141–157 (2004).
53. J. De Gelder et al., "Reference database of Raman spectra of biological molecules," *J. Raman Spectrosc.* **38**(9), 1133–1147 (2007).
54. N. Stone et al., "Near-infrared Raman spectroscopy for the classification of epithelial pre-cancers and cancers," *J. Raman Spectrosc.* **33**(7), 564–573 (2002).
55. W. T. Cheng et al., "Micro-Raman spectroscopy used to identify and grade human skin pilomatricoma," *Microsc. Res. Tech.* **68**(2), 75–79 (2005).
56. H. Han et al., "Analysis of serum from type II diabetes mellitus and diabetic complication using surface-enhanced Raman spectra (SERS)," *Appl. Phys. B* **94**(4), 667–672 (2009).
57. P. Andrade et al., "Study of normal colorectal tissue by FT-Raman spectroscopy," *Anal. Bioanal. Chem.* **387**(5), 1643–1648 (2007).
58. N. Stone et al., "Raman spectroscopy for early detection of laryngeal malignancy: preliminary results," *Laryngoscope* **110**(10), 1756–1763 (2000).
59. J. Binoy et al., "NIR-FT Raman and FT-IR spectral studies and ab initio calculations of the anti-cancer drug combretastatin-A4," *J. Raman Spectrosc.* **35**(11), 939–946 (2004).
60. J. W. Chan et al., "Micro-Raman spectroscopy detects individual neoplastic and normal hematopoietic cells," *Biophys. J.* **90**(2), 648–656 (2006).
61. D. P. Lau et al., "Raman spectroscopy for optical diagnosis in the larynx: preliminary findings," *Lasers Surg. Med.* **37**(3), 192–200 (2005).
62. J. R. Perno, C. A. Grygon, and T. G. Spiro, "Ultraviolet Raman excitation profiles for the nucleotides and for the nucleic acid duplexes poly (rA)-poly-(rU) and poly (dG-dC)," *J. Phys. Chem.* **93**(15), 5672–5678 (1989).
63. Z. Huang et al., "Near-infrared Raman spectroscopy for optical diagnosis of lung cancer," *Int. J. Cancer* **107**(6), 1047–1052 (2003).
64. F. Banki et al., "Plasma DNA is more reliable than carcinoembryonic antigen for diagnosis of recurrent esophageal cancer," *J. Am. Coll. Surg.* **207**(1), 30–35 (2008).

65. R. Gebhard et al., "Abnormal cholesterol metabolism in renal clear cell carcinoma," *J. Lipid Res.* **28**(10), 1177–1184 (1987).
66. M. H. Hager, K. R. Solomon, and M. R. Freeman, "The role of cholesterol in prostate cancer," *Curr. Opin. Clin. Nutr. Metab. Care* **9**(4), 379–385 (2006).
67. L.-B. Wang et al., "Amino acid uptake in arterio-venous serum of normal and cancerous colon tissues," *World J. Gastroenterol.* **10**(9), 1297–1300 (2004).
68. P. L. Alo et al., "Expression of fatty acid synthase (FAS) as a predictor of recurrence in stage I breast carcinoma patients," *Cancer* **77**(3), 474–482 (1996).
69. D. K. Nomura et al., "Monoacylglycerol lipase regulates a fatty acid network that promotes cancer pathogenesis," *Cell* **140**(1), 49–61 (2010).
70. M. S. Shurbaji, J. H. Kalbfleisch, and T. S. Thurmond, "Immunohistochemical detection of a fatty acid synthase (OA-519) as a predictor of progression of prostate cancer," *Hum. Pathol.* **27** (9), 917–921 (1996).
71. N. Burns-Cox et al., "Changes in collagen metabolism in prostate cancer: a host response that may alter progression," *J. Urol.* **166**(5), 1698–1701 (2001).

Sevda Mert is currently a PhD student in the Genetics and Bioengineering Department of Yeditepe University, Turkey, Istanbul. She holds an MSc degree in biotechnology, and her current research

interest is the utility of SERS and Raman spectroscopy for diagnostic applications.

Emin Özbek is an associate professor at Istanbul Samatya Training and Research Hospital. He received his MD degree from Karadeniz Technical University School of Medicine. He completed his residency at Ege University.

Alper Ötünçtemur is an associate professor of clinical urology. He received his MD degree from Cerrahpasa University School of Medicine. He completed his urology residency at Vakıf Gureba Training and Research Hospital University. Currently, he is in the Department of Urology at Okmeydanı Training and Research Hospital. His clinical interests include all areas of urologic oncology.

Mustafa Çulha obtained his PhD degree in chemistry from the University of Tennessee-Knoxville in 2002 and joined the Advanced Biomedical Research Group as a postdoctoral researcher at Oak Ridge National Laboratory (2002–2003) before joining the Schering-Plough Corporation. In 2004, he accepted a faculty position in the Genetics and Bioengineering Department of Yeditepe University, Turkey. His research focuses on development of novel detection and diagnostic tools using spectroscopic techniques such as surface-enhanced Raman scattering for medical and biomedical applications.